Microstructure modelling for metallic additive manufacturing : a review

Tan, Joel Heang Kuan; Sing, Swee Leong; Yeong, Wai Yee

2020

Tan, J. H. K., Sing, S. L., & Yeong, W. Y. (2020). Microstructure modelling for metallic additive manufacturing : a review. Virtual and Physical Prototyping, 15(1), 87-105. doi:10.1080/17452759.2019.1677345

https://hdl.handle.net/10356/145915

https://doi.org/10.1080/17452759.2019.1677345

Microstructure Modelling for Metallic Additive Manufacturing: A Review

The microstructure of metal built using AM is highly dependent on the process parameters. However, experimentation on different process parameters for different materials is costly and time consuming. To overcome these challenges, numerical simulations provide insights that allow prediction of microstructure formed under different process parameters. Microstructure modelling requires coupling of macro-scale thermal model or experimentally measured temperature profiles with either a meso-scale or micro-scale microstructure model. In this review, the commonly used AM techniques for metals are introduced, followed by discussion on the microstructure of parts fabricated using these processes. This review then presents the latest models used in simulating different microstructural aspects of metal AM parts. In addition, the models were compared and the potential and challenges in microstructure modelling were discussed.

Keywords: additive manufacturing; simulation; microstructure; numerical model; 3d printing

1 Introduction

Additive manufacturing (AM) is a group of manufacturing methods to produce highly customized parts catering to the low volume markets (Chua and Leong 2017). According to ISO/ASTM 52900:2017, AM is the general term for those technologies that based on a geometrical representation creates physical objects by successive addition of material. AM involves process of joining materials to make parts from 3D model data, usually layer upon layer, as opposed to subtractive manufacturing and formative manufacturing methodologies. AM is able to build complex geometries without the need for moulds potentially reducing part count (Gibson, Rosen et al. 2010, Atzeni and Salmi 2012). The aerospace and healthcare industries can use AM to their advantage with metals like stainless steel, titanium, cobalt chrome and nickel alloys (Vandenbroucke and Kruth 2007, Brunette, Tengvall et al. 2012, Cantor, Assender et al. 2015). While AM can achieve complex geometry, the manufacturing process is highly complex with numerous

factors affecting the properties of the part. An important feature of metal is its microstructure. For a given metal there can be a variety of microstructural features that affects its mechanical properties. The size of grains, microsegregation of alloying elements, phases within the metal and size of dendrites relates to the tensile strength and ductility (Warren and Boettinger 1995, Lu, Luo et al. 2010). During the AM process, the microstructure is formed *in-situ* and would therefore depend largely on the process parameters and material used. The process parameters are dependent on the metal AM method used.

1.1 Additive Manufacturing Methods

There are two broad techniques in additive manufacturing of metals, powder bed fusion (PBF) and directed energy deposition (DED). PBF process includes selective laser sintering (SLS), selective laser melting (SLM) and electron beam melting (EBM). SLM and EBM are used for fabrication of metals.

Both processes start from digital files. 3D computer-aided design (CAD) files are sliced into layers and the data is sent to the machine for printing. The next step is a set of cycles that melts the powders layer by layer till the final product is completed. In each cycle, a fixed thickness of powder is deposited onto a substrate and a heat source is applied to the powder in a raster scanning pattern. This melts the layer of powder, bonding it to the substrate or to the previously melted layer. Lastly, the platform is lowered and the cycle repeats. The heat source could either be laser or electron beam.

DED processes on the other hand can use wire or powder as the feedstock, and energy sources could use laser, electron beam and electricity for wire feedstock. As DED machines can have 5 axis of movement, the layer addition to the CAD file may need to be sliced in a computer aided manufacturing (CAM) software. Energy source could be applied to the feedstock coaxially or off axis. The feedstock is melted close to the

substrate or on the substrate forming a layer. Examples of SLM and coaxial laser direct energy powder deposition setups are shown in **Figure 1**.

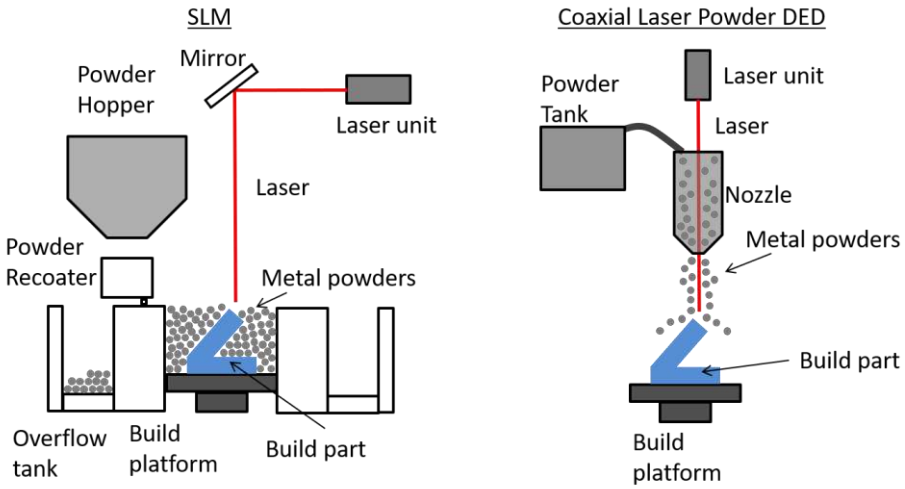

Figure 1. Schematic of selective laser melting and coaxial laser directed energy powder deposition.

While both PBF and DED processes build the part layer by layer, there can be distinct differences between the two. PBF machines are currently limited to 3 axis systems forcing layers to build up in a single direction. DED machines can have 5+ axis systems allowing layers to be built in any direction provided there is no clashing of the part and tool head. This allows DED to be a better process for repairing parts using AM. Parts produced by PBF can have better resolution due to the smaller powder size and smaller energy spot size as compared to DED machines. Parts made by PBF may not require as much post processing than parts made from DED. The larger powder size or using wires lead to more material deposited in the DED process leading faster build speeds but lower tolerance and resolution. This may lead to parts made using DED requiring to be cut to size, increasing cost and time in the post processing.

1.2 Microstructure of Additive Manufactured Metals

AM processes have been used to print certain alloys like 316L stainless steel, Ti-6Al-4V and Inconel 625/718 which are common alloys used in marine and aerospace applications. The microstructure of metals determines the mechanical properties of the part such as yield strength, ductility and hardness (Peel, Steuwer et al. 2003, Ziętala, Durejko et al. 2016, Guo, Zou et al. 2017, Shuai, Xue et al. 2018). AM process predominantly produces columnar grains with a mix of equiaxed grains that consist of cellular dendrites (**Figure 2**) (Murr, Gaytan et al. 2012, Frazier 2014, Roehling, Wu et al. 2017). The columnar grains typically grow along the build direction causing anisotropy and difference in performance in varying build orientations (Lewandowski and Seifi 2016). By varying the process parameters like the energy sources and feed types can lead to differences in grain structure (Frazier 2014). Ti-6Al-4V had columnar grains when printed with multiple tracks using electron beam-wire-DED and laser-powder-DED, however, when printed using laser-powder-DED for a single track the grains do not grow in a columnar fashion. The Ti-6Al-4V microstructure was finer in the electron beam-wire-DED as compared to the laser-powder-DED (Murr, Gaytan et al. 2012, Dehoff, Kirka et al. 2015). Ti-6Al-4V was shown to exhibit near equiaxed prior-beta grains that quickly grow to large columnar grains after the initial layers, indicating that varying cooling rates and temperature gradient can induce changes in microstructure (Tan, Kok et al. 2015). The cooling rate and temperature gradient also affects dendritic formation. Cellular dendrites are formed when the cooling is fast, while slower cooling rates allow formation of secondary dendrite arm (Kou 2003). High cooling rate and low temperature gradient can cause an increase in mechanical properties, like in the case of Inconel 718 where the finer distributed laves phases are formed, leading to lesser chance of hot cracking (Nie, Ojo et al. 2014). As the grain structure and dendrites affects the overall mechanical properties, it is important to

know how different printing techniques and process parameters affects the grain structure (Gifkins 1976, Baufeld, Van der Biest et al. 2010).

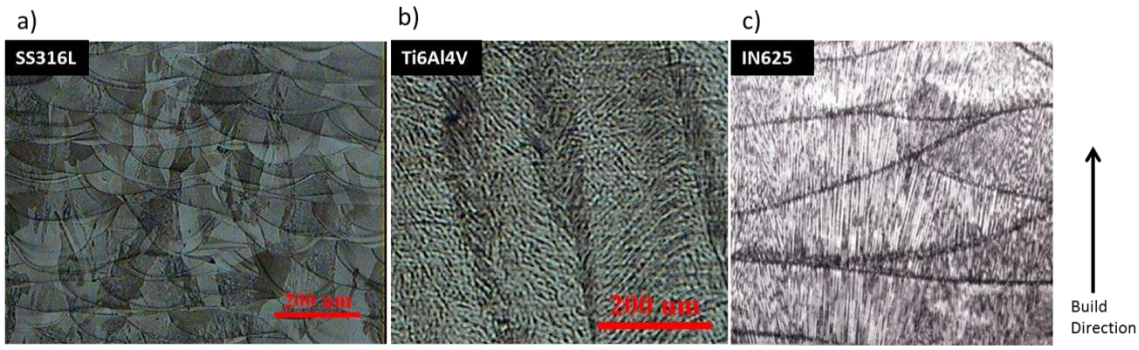

Figure 2. Columnar grains observed in various additive manufactured metal alloys; a) 316L stainless steel, b) Ti6Al4V and c) Inconel 625, "Comparison of microstructures and properties for a Ni-base superalloy (Alloy 625) fabricated by electron and laser beam melting" by K. Amato *et al.* is licensed under CC BY 4.0 (Amato, Hernandez et al. 2012).

The microstructure of metals depends largely on the thermal gradient and cooling rate during solidification. By varying the process parameters, it is possible to alter the grain structure. Raghavan *et al.* used two different scanning strategies, one with line scans and another spot scanning. Line scans tend to cause columnar grains while spot scanning together with controlling of the current, duration and distance between each spot lead to more equiaxed grains being formed (Raghavan, Dehoff et al. 2016). Dehoff *et al.* additionally alternate line and spot scanning within the same part to achieve different areas with columnar and equiaxed grains. The sequence in which the boundary area, equiaxed area and columnar area is printed first also matters as it affects the temperature gradient (Dehoff, Kirka et al. 2015). In both cases, EBM is used and had the powder bed pre-heated to near melting temperature of the material, this helps lower the overall temperature gradient allowing equiaxed grains to form.

It is shown that changing the parameters and scanning strategy can result in tailored microstructure (Körner, Helmer et al. 2014, Parimi, Ravi et al. 2014, Dehoff, Kirka et al. 2015, Wei, Mazumder et al. 2015, Raghavan, Dehoff et al. 2016). Tailored microstructure

can help in applications that require texture or the lack of it like in single crystal turbine blades and provide possibilities in grain boundary engineering.

Transition of columnar to equiaxed grains depends largely on the temperature gradient as well as the cooling rate. These values can be found experimentally or computer simulations. Experimental methods can only investigate microstructure after the entire part is printed. *In-situ* monitoring of the AM process have limited capabilities and are restrained to monitor surface effects, and provide no information beyond the surface (Clijsters, Craeghs et al. 2014, Huang, Leu et al. 2015, Everton, Hirsch et al. 2016, Lu and Wong 2018).

Computer simulation of the AM process helps in understanding the evolution of temperature beyond the top surface. Simulations uses the temperature results from thermal models to predict microstructure on varying length scales. As AM process involves building layer upon layer, the melt tracks experience multiple remelting. Experimental data can only give the grain structure after the entire build, while simulation provides access to the evolution of the grain structure throughout the process. The aim of the paper is to review the different methods of microstructure modelling used specifically for AM metals. The different microstructure models are compared, and their strengths and limitations are explored.

2 Modelling for Metal Additive Manufacturing

Modelling of microstructure requires coupling models at different length scales. First, a macro-scale thermal model is required to get the thermal history of the part during the AM process. Simulation of the thermal model can range from a single melt track to multiple melt tracks and across multiple layers. Second, data from the thermal model is used as input to the microstructure model. Microstructure models can be further categorised based on another length scale, meso-scale and micro-scale. Meso-scale

simulation refers to models that simulate for multiple grains, while micro-scale simulation refers to models that simulate the dendritic formation.

2.1 Thermal Modelling in Additive Manufacturing

Thermal numerical models can investigate the temperature the material would experience during the AM process. Thermal models can predict the temperature profile, fluid flow, porosity and be coupled to microstructure models or thermo-mechanical models to get the microstructure or residual stress and deformation (Vastola, Pei et al. , Denlinger, Heigel et al. 2015, Yang, Jamshidinia et al. 2018). The temperature profile could also be used to get predict the amount of precipitate formed, columnar grain growth orientation and CET (Liu, Zhu et al. 2018, Yin, Peng et al. 2018, Kumara, Segerstark et al. 2019). Microstructure modelling uses thermal models to find the temperature history and shape of the scanned tracks as input. This section reviews the thermal models used in conjunction with microstructure models.

2.1.1 Finite Difference Method and Finite Element Method

Finite difference method (FDM) and finite element method (FEM) have been coupled with various microstructure models, typically simulating for large volumes of multiple tracks and layers (Mercelis and Kruth 2006, Zeng, Pal et al. 2015, Chen, Guillemot et al. 2016, Zinovieva, Zinoviev et al. 2018). FEM/FDM solves for the heat equation partial differential equation (PDE):

$$\rho c_p \frac{\partial T}{\partial t} - \nabla \cdot (k \nabla T) = Q_s \,. \tag{1}$$

In Equation 1, ρ is the density, c_p is the specific heat capacity, T is the temperature, t is the time, k is the thermal conductivity and Q_s is the heat source added to the model. Heat loss by radiation and convection is sometimes added to the top surface as boundary conditions (Loh, Chua et al. 2015).

Simulating for PBF, FEM models often uses elements of different materials. The top elements are assigned as the powder material and the remaining elements are the substrate material (**Figure 3**a). The powder element often has the density based on the porosity of the powder bed multiplied by the substrate density. The thermal conductivity is similarly dependent on the porosity of the powder bed (Chen, Guillemot et al. 2016, Foroozmehr, Badrossamay et al. 2016, Chiumenti, Neiva et al. 2017). Elements that are assigned as powder material would change to substrate material once the temperature of the element goes above the liquidus temperature. Simulating for DED differs slightly from PBF models. Material has to be added while the heat source moves. FEM models do this by first placing dead/inactive elements above the substrate, as the heat source moves, the dead/inactive elements are set to be alive/active (**Figure 3**b) (Fallah, Alimardani et al. 2011). This simulates the material being fed and added to the melt pool. Dead/inactive elements work by having its thermal conductivity set to near zero such that the temperature of the element would not change.

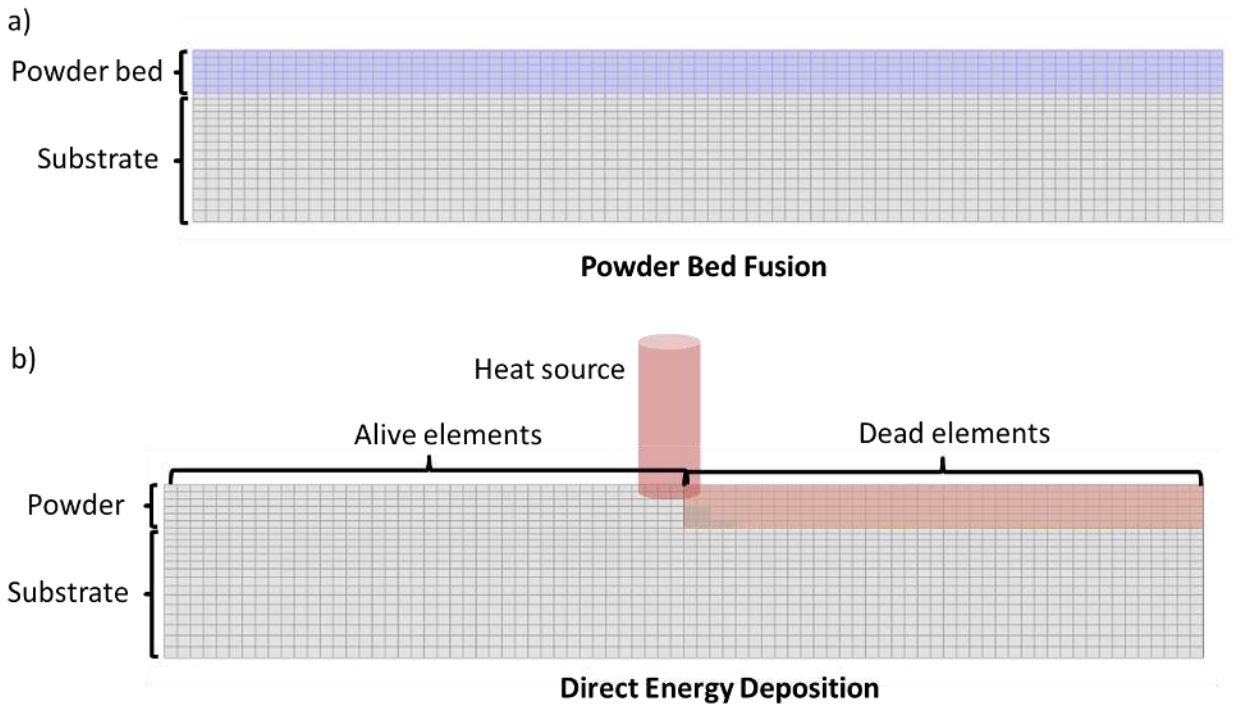

Figure 3. Representation of FEM for a) Powder bed fusion showing the top element is set to powder material while the rest is set to fully dense material and b) laser direct energy deposition with powder material set to dead/inactive that change to alive/active elements when the heat source reaches it.

Meshing for FEM plays an important role in getting accurate temperature profiles and melt depths. Hexahedral element is commonly used as it provides better accuracy and works well with simple geometry used in simulations (Lindgren, Häggblad et al. 1997, Yin, Peng et al. 2018). AM processes have localised areas of large temperature changes at the area of the heat source. Chiumenti et al. suggested that in order to have better estimation of the temperature, the elements size have to be smaller than the energy source spot size, Foroozmehr *et al.* used eight by eight elements within the laser spot (Foroozmehr, Badrossamay et al. 2016, Chiumenti, Neiva et al. 2017). Having high resolution throughout the entire mesh can lead to long computational time. As such, most models simulate for a single melt track. In order to simulate for a larger volume, Patil *et al.* used adaptive mesh refinement (AMR) to have higher resolution in and around the melt pool and progressively coarser mesh beyond the melt pool leading to an decrease in computing time by a hundred times (Patil, Pal et al. 2015). This allows solving for a larger

area allowing investigations on scanning strategies involving simulating for multiple tracks. Denlinger used a similar method and found it to be 432 times faster than using static mesh (Denlinger 2018).

2.1.2 Computational Fluid Dynamics

Computational fluid dynamics (CFD) methods like the finite volume method (FVM) have been used to get the shape of the track, melt pool and the temperature history. FVM methods are used to solve the Navier-Stokes equation which can simulate effects like vaporization and Marangoni effect seen in AM (Khairallah, Anderson et al. 2016, Andani, Dehghani et al. 2017). This would lead to higher accuracies in the temperature distribution in the melt pool and also higher accuracies in geometry (Khairallah, Anderson et al. 2016). In order to simulate the fluid flow within the melt, the mass and momentum equation have to be included alongside the energy equation (Gürtler, Karg et al. 2013, Yuan and Gu 2015):

$$\frac{\delta}{\delta t}(\rho H) + \nabla \cdot (\rho \vec{v} H) - \nabla \cdot (k \nabla T) = Q_S, \tag{2}$$

$$\frac{\delta \rho}{\delta t} + \nabla \cdot (\rho \vec{v}) = M_s, \tag{3}$$

$$\rho \frac{\delta \vec{v}}{\delta t} + \rho \vec{v} \cdot \nabla \vec{v} = -\nabla p + \mu \Delta \vec{v} + M_s \vec{v} + F. \tag{4}$$

Equation 2 is the energy equation for heat conduction where H is the enthalpies and $\vec{v}$ is the velocity of fluid. Equation 3 is the mass conservation equation where M_s is the mass source. In PBF where powders are already laid before simulating, the mass source can be considered as zero while in DED where powders are added while running would require

the mass source term. Equation 4 is the momentum equation where μ is the dynamic viscosity and F is a force term like gravitational force that may be included. The increase in the number of PDEs needed to solve leads to increase of computing power required. Most FVM models only simulate a single melt track in 3D (Fallah, Amoorezaei et al. 2012, Lee and Zhang 2015, Khairallah, Anderson et al. 2016, Panwisawas, Qiu et al. 2017). CFD of PBF can use varying type of powder distribution, either by powder packing density or using numerical models like discrete element method (DEM) (Lee and Zhang 2015, Zielinski, Vervoort et al. 2017). Numerical methods of packing powder led to irregular powder distribution that is closer resembling to actual powder deposition in PBF processes. CFD-DEM method has been used for DED processes as well, taking into account of gas flow, powder flight and heating as well as interactions with the melt pool (Pinkerton 2015). The amount of details required of the simulation causes it to be even more computationally expensive as DEM is simulated together with CFD and gas flow has to be taken into account as well. While CFD can lead to more realistic tracks, literature of using CFD for DED processes is few.

The lattice Boltzmann method (LBM) is another CFD method that is used to couple with microstructure models. LBM does not solve the Navier-Stokes equation, instead, it solves discrete Boltzmann equations to model the fluid flow (Rausch, Küng et al. 2017). LBM can simulate the powder distribution as well as the fluid flow and evaporation while FVM would require coupling with discrete element method to simulate the powder distribution (Khairallah, Anderson et al. 2016, Liu and Wang 2017). LBM becomes comparatively more expensive when changing from 2D to 3D, with most 2D models being able to simulate for multiple layers for a single track, a 3D model however, can simulate for multiple tracks in a single layer (Körner, Bauereiß et al. 2013, Rai, Markl et al. 2016,

Degenhardt 2017). LBM have been used to model PBF processes however no literature was found to have used LBM for DED processes at the time of writing.

CFD models have an average cell size of 5 µm and average domain of 150x1000x150 µm (Körner, Bauereiß et al. 2013, Lee and Zhang 2015, Zielinski, Vervoort et al. 2017). In comparison, FEM models have element size ranging from 25 µm to 5 mm and domain size ranging from 0.4x1x0.4 mm to 250x250x325mm (Loh, Chua et al. 2015, Foroozmehr, Badrossamay et al. 2016, Chiumenti, Neiva et al. 2017). The model and element size can differ by three orders of magnitude. The number of cells for CFD also range in the millions while FEM elements tend to be less than a million. While CFD models can simulate multiple physical phenomena, the complexity and small cell size limits the total domain to be less than a millimetre in length, limiting the simulation to few short tracks. FEM models have many assumptions, reducing accuracy but increasing the size of the domain to accommodate multiple longer tracks and multiple layers.

2.2 Microstructure Modelling in Additive Manufacturing

There are similarities between melting of a single track in AM and welding. Welding typically adds material between two metal parts thereby joining them while AM adds material to a substrate or previously printed layer. The solidification of both welding and AM are very similar since both uses a moving heat source to melt the added material leading to a moving melt pool. Since welding research is more developed, microstructure modelling techniques in welding can be applied and translated to AM (Seufzer 2014, Rolchigo, Mendoza et al. 2017).

There are three microstructure models that are reviewed, phase field modelling (PFM), kinetic Monte Carlo (MC) and cellular automata (CA). CA and MC are considered meso-scale models as they simulate multiple grains mainly looking at the overall size and aspect ratio of the grains. PFM is considered a micro-scale model as it can simulate on the sub-

grain level, getting the solute concentration, precipitates and dendrites shape. It is also able to simulate for multiple grains using multi-phase field models (Miyoshi, Takaki et al. 2019).

The coupling between macro thermal model and the microstructure model can be done in two ways. The models can be weakly coupled, where the thermal model is simulated first and the thermal history is used as input to the microstructure model. Another way is to strongly couple them and simulate both at the same time, where information is shared and interacts between both models. Although strongly coupled simulations would be able to yield more accurate results, it requires longer computational time (Gandin, Desbiolles et al. 1999). A schematic of the different microstructure models is shown in Figure 4 showing the boundary conditions and assumptions of the model.

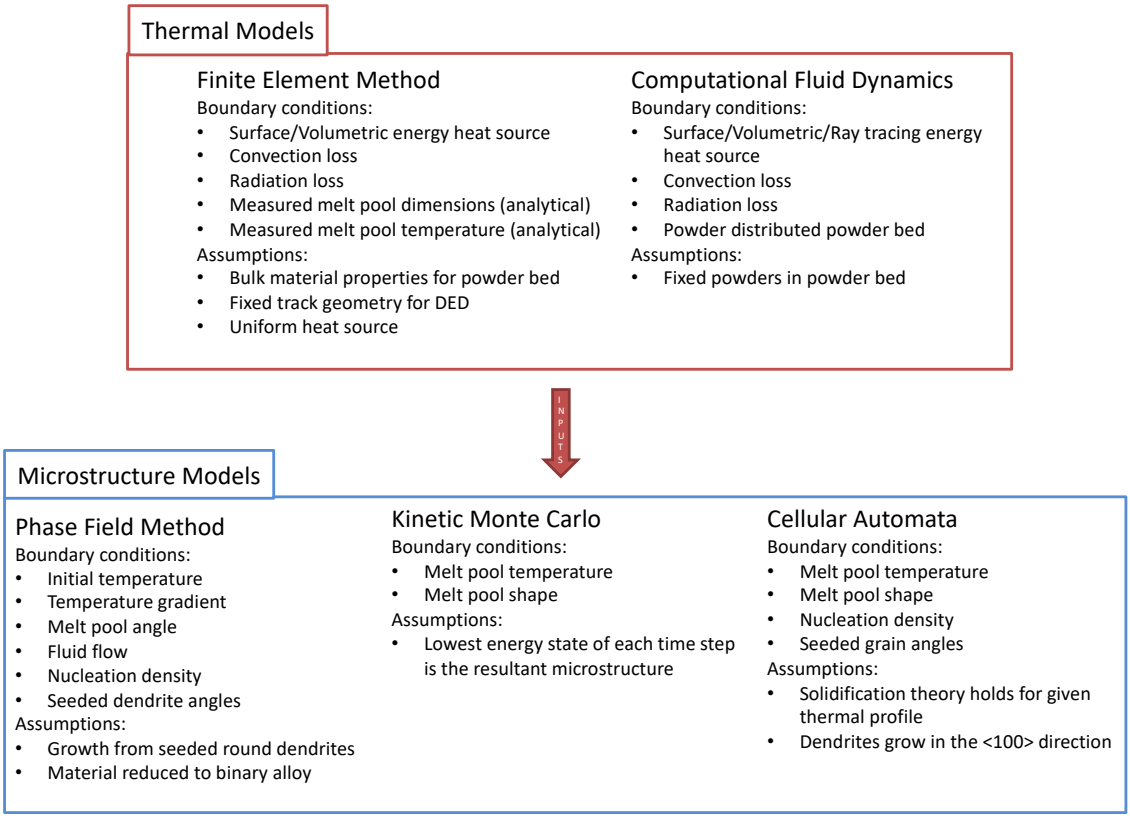

Figure 4 Schematic of thermal and microstructure models with their boundary conditions and assumptions.

2.2.1 Phase Field Modelling

Phase field modelling (PFM) has been shown to be able to model solid, liquid and material phases within the same model. Microstructure evolution like grain coarsening and dendrite growth in forced convection could be simulated as well (Gránásy, Pusztai et al. 2004, Singer-Loginova and Singer 2008, Sahoo and Chou 2014). PFM is thermodynamically consistent, however, the interface width has to be thin in PFM increasing difficulty in modelling thereby limiting the size of the model (Elder, Grant et al. 2001). A large model with several interfaces will be too computationally expensive to run, especially if it is in 3D. While PFM provides the ability to simulate multiple phenomena with high accuracy, computational resources will be limiting factors (Francois, Sun et al. 2017).

2.2.1.1 Phase Field Modelling Theory

PFM simulates microstructures by having all variables to be continuous across the interface. The interface can be a fraction of both solid and liquid. Mathematically, the description of the interface or otherwise called the phase field variable, ϕ, can be represented as $\phi \in [-1,1]$. During the solidification process, the system of a fixed volume would tend towards a lower free energy in order to achieve stability (Boettinger, Warren et al. 2002, Kim and Kim 2005, Steinbach 2009):

$$F = \int [f(\phi, c, T) + \omega g(\phi) + \epsilon^2 |\nabla \phi^2|] dV \,, \tag{5}$$

where F is the total free energy of the system, f is the thermodynamic potential, c is the concentration, $\omega g(\phi)$ is the double well potential, $\epsilon^2 |\nabla \phi^2|$ is the phase field gradient energy and V is the volume. The phase field gradient energy is dependent on the gradient of the interface and therefore would be zero in fully solid and liquid regions. The thermodynamic potential is the sum of the free energies of the liquid and solid states.

Over time, the system would decrease the total free energy of system. In order to solve the transient problem, the Allen-Cahn and Cahn-Hilliard equations can be used (Boettinger, Warren et al. 2002, Chen 2002, Kim and Kim 2005):

$$\frac{\partial \phi}{\partial t} = -M_\phi \left[\frac{\partial f}{\partial \phi} + \omega g'(\phi) - \epsilon^2 \nabla^2 \phi\right], \tag{6}$$

$$\frac{\partial c}{\partial t} = \nabla \cdot M_c \nabla \frac{\partial f}{\partial c}, \tag{7}$$

where M_ϕ and M_c are the motilities of the phase field and concentration field at the interface respectively. In a multiphase problem like in solidification of certain steels, there can be liquid, ferrite and austenite, each of these phases have its own variable, $\phi_i(\vec{x}, t)$ where i denotes the state that the field is. The sum of the phases in a multiphase system has to reach unity, $\sum_{i=1}^{N} \phi_i = 1$ (Boettinger, Warren et al. 2002).

2.2.1.2 Application of Phase Field Modelling

Farzadi *et al.* used CFD and PFM to simulate the growth of columnar dendrites in the Al-Cu weld to investigate the solute concentration, dendrite arm spacing and undercooling at varying welding speed (Farzadi, Do-Quang et al. 2008). The method used can be applied to the scanning of a single track in AM for binary alloys. Montiel *et al.* used 2D PFM to investigate the CET of magnesium alloy during welding (Montiel, Liu et al. 2012).

FEM and PFM have been coupled to simulate for AM processes. The temperature gradient and cooling rates were found using FEM and used as boundary condition in PFM. Gong and Chou simulated in 2D for EBM of Ti6Al4V using FEM and PFM (Gong and Chou 2015). The thermal model show that faster scanning speeds led to higher cooler,

the cooling rate is used to find the distance between seeds for the PFM models too. The PFM model showed columnar prior beta grains which grew faster with higher cooling rates and experimental results showed similar prior beta grain sizes. However, the grain size was partially affected by the predetermined distance between seeds. Sahoo and Chou found the grain size differently, simulating from a single dendrite and using the primary dendrite arms spacing as the grain size (Sahoo and Chou 2016). Sahoo and Chou simulated the EBM process using a thermal model in 3D and a PFM model in 2D. A single dendrite was simulated and its primary dendrite arms grew in the columnar fashion and was compared to the experimental results showing columnar grains. The primary dendrite spacing and arm width was found to get smaller as scanning speed increases. The simulated dendrite arm spacing was larger than experimental results by approximately 0.5 µm. Within a melt pool, the solid-liquid interface can have different temperature gradient and solidification velocity at the bottom and trailing edge of the melt pool. Fallah *et al.* simulated for laser powder DED of Ti-Nb using 3D FEM to find the localised temperature gradient and solidification velocity which is input to 2D PFM models (Fallah, Amoorezaei et al. 2012). The thermal model found that the temperature gradient is smaller and the solidification velocity faster near the surface as compared to the bottom. PFM models for different temperature gradient and solidification velocity was simulated and the dendrite spacing was compared to experimental results. The PFM model was accurate except at the extreme ends where temperature gradient or solidification velocity is highest. Different PFM model or boundary conditions may need to be applied to get more accurate results. CFD can simulate the Marangoni flow which enhances cooling and thus can get more accurate melt pool shape and temperature profile, Acharya *et al.* simulated with SLM process for Inconel 718 using 2D PFM with the domain shaped like the melted track found using 3D CFD (Acharya, Sharon et al. 2017).

Although CFD was used, the PFM model had some differences with experimental results. The primary dendrite spacing and segregation of solutes tally with experimental results, however, the simulated results show secondary dendrites growing while experimental results show little to no secondary dendrites. All the PFM models reviewed reduced the complexity by simplifying the alloys to binary alloys.

2.2.2 Kinetic Monte Carlo

Kinetic Monte Carlo (MC) modelling is a completely probabilistic simulation of the grain structure. MC is able to simulate grain structures over large volumes due to the low computational resource required. MC models differ from PFM models which simulate the solute concentration and dendrite shape, MC only models the grains therefore simulating on a different length scale. MC models provide the shape and size of grains.

2.2.2.1 Kinetic Monte Carlo Theory

The MC method is based on an atomistic simulation and the minimization of the overall system energy. Each site on the lattice is given a number or orientation and if the neighbour of a site has a different orientation, it would add to the overall system energy. If the neighbour has the same orientation, there is no change in the system energy. Each site has a probability of changing orientation, if the orientation contributes to a decrease in the overall energy system, then it is accepted. If the change in orientation causes an increase, a random number would generate for that site and compare to an acceptance probability and if the random number is smaller than the acceptance probability, it is accepted. These are shown in the following (Yang, Sista et al. 2000, Rodgers, Madison et al. 2017):

$$\Delta E = J \sum \left[1 - \delta\left(I_{j,} I_k\right)\right], \tag{8}$$

$$P = \begin{cases} exp\,(\frac{-\Delta E}{k_B T_0}), & \Delta E > 0 \\ 1, & \Delta E \leq 0 \end{cases}, \quad (9)$$

where ΔE is the overall system energy, J is a scaling factor of the energy system, δ is the Kronecker delta function, lattice assigned number or spin,$I_{j,} I_k$ are the number/spin of the site and neighbour, k_B is the Boltzmann's constant and T_0 is the ambient temperature of the process. This happens within a MC time step, every time step the lattice is taken as-is and every site is recalculated and compared with the previous time step. In general, if the current step has an increase in overall energy, it is rejected and the previous time step configuration is kept. In order to simulate solidification, some modifications to the MC method have to be made. The grain boundary mobility is dependent on the temperature at the site and follows the Arrhenius equation (Yang, Sista et al. 2000, Rodgers, Madison et al. 2017). Equation 9 is then modified to:

$$P = \begin{cases} [M_0 exp\,(\frac{-Q_{act}}{R_{gas} T})] exp\,(\frac{-\Delta E}{k_B T_0}), & \Delta E > 0 \\ M_0 exp\,(\frac{-Q_{act}}{R_{gas} T}), & \Delta E \leq 0 \end{cases}, \quad (10)$$

where M_0 is the Arrhenius pre-exponential factor, Q_{act} is the activation energy, R_{gas} is the gas constant and T is the site temperature. MC method requires relatively lower computational resources and is able to simulate both 2D and 3D (Stefanescu 2015). It is able to simulate multiple laser passes and layers due to the low computation cost (Rodgers, Madison et al. 2017). MC models are able to capture the overall grain structure shapes and sizes but it does not take into account the preferential crystallographic growth direction, which would affect final grain shapes and angles.

2.2.2.2 Application of Kinetic Monte Carlo

MC methods have been used to simulate microstructure for casting, sintering and welding. It is also able to model the change of microstructure during recrystallization and grain growth (Zhong 2011, Liu, Cheng et al. 2014). Mishra and DebRoy used MC to predict grain sizes in the heat affected zone (HAZ) due to solidification and grain growth in Ti6Al4V during welding (Mishra and DebRoy 2004, Mishra and DebRoy 2004). The models showed potential to be used for simulating repairs using AM, especially to treated metal, that leads to HAZ. Thermal models are also coupled with MC to predict grain structures in welding (Yang, Sista et al. 2000, Wei, Elmer et al. 2017). Wei *et al.* capture the aspect ratio and grain sizes at varying welding speeds of aluminium alloys using CFD and MC. However, the model was not validated against experimental data (Wei, Elmer et al. 2017).

Rodgers *et al.* predicted the 3D microstructure in a single pass electron beam welding using MC and later increasing the number of scans extending it to EBM and electron beam powder DED (Rodgers, Madison et al. 2016, Rodgers, Madison et al. 2017). The model was able to simulate a large volume capturing the crystal growth bias towards the scanning direction. While the model was able to capture the patterns the experimental EBSD data, the aspect ratio and sizes are not fully captured. Sun *et al.* used different melt pool geometry in MC for the solidification of 316L and found equiaxed grains growing in the middle of the track for fast scanning speed (Sun, Tan et al. 2018). The results support experimental data that columnar grains being broken off each layer at faster scanning speed. However, the grain size and aspect ratio also differ from experimental data. While the MC method has been used extensively for welding, the use of it for AM is few. MC method, however, has the least computational cost and has the potential to model over large volumes.

2.2.3 Cellular Automata

Cellular automata (CA) simulation is a probabilistic model with deterministic elements in it. The nucleation rate and dendrite direction are probabilistic while the growth of dendrites and preferential crystallographic direction is taken from theory. Similar to MC, CA simulates the grain structure rather than the dendrites. Having more equations to solve, CA uses more computational resources than MC but is able to capture grain angles and grow accordingly. This can lead to more accurate results.

2.2.3.1 Cellular Automata Theory

CA uses certain rules to change the state of a cell and in the case of solidification, the states are solid, liquid and mushy. CA requires a mesh of equally divided cells, usually square (2D) or cube shape (3D), with each cell interactive with its neighbouring cells by the rules. The CA model would require rules that govern the transition from solid to liquid, liquid to solid, setting of crystallographic orientation, speed and orientation of capturing neighbouring cells for crystal growth. CA follows rules of solidification theory as well as some probability elements for nucleation. CA models are often coupled with macro thermal models to help in the rules of solid-liquid transition. CA models are like MC models in that both do not calculate the dendritic structures like secondary arm growth but instead simulate the grain structure allowing it to capture a larger scale. The changing of cell state from liquid to solid depends not only on temperature but the probability of nucleation as well. CA models use a probabilistic approach to determine nucleation, as undercooling, ΔT, drives the solidification, the continuous grain density, n, is given by (Gandin and Rappaz 1994):

$$n(\Delta \mathrm{T}) = \int_0^{\Delta T} \frac{dn}{d(\Delta T)} d(\Delta T)\,. \tag{11}$$

A Gaussian distribution can be used to determine if a cell forms a nucleus:

$$\frac{dn}{d(\Delta T)} = \frac{n_{max}}{\sqrt{2\pi}} \exp\left[-\frac{(\Delta T - \Delta T_{mean})^2}{2\Delta T_\sigma}\right], \quad (12)$$

where n_{max} is the maximum nucleation density, ΔT is the undercooling of the liquid, ΔT_{mean} is the mean undercooling when nucleation occurs and ΔT_σ is the standard deviation of the undercooling. Capturing of neighbouring cells by crystal growth is determined by solidification theory. One of the growth kinetics models is the KGT model. The KGT model assumes that the solid-liquid interface would grow at near absolute stability limit and the velocity can be found as a function of the undercooling (Kurz, Giovanola et al. 1986):

$$\Omega = \frac{C^* - C_0}{C^*(1-K)} = Iv(\frac{VR}{2D}), \quad (13)$$

$$R = 2\pi \sqrt{\frac{\Gamma}{mG_c\xi_c - G}}, \quad (14)$$

$$\xi_c \approx \frac{\pi^2}{K\frac{VR}{2D}_2}, \quad (15)$$

$$\Delta T = mC_0(1 - \frac{1}{\Omega(1-\mathrm{K})}), \quad (16)$$

where Ω is the solute supersaturation, C^* is the liquid solute concentration at the tip of the dendrite, C_0 is the initial solute concentration, D is the solute diffusion coefficient, K is the partition coefficient, R is the radius of the tip of the dendrite, m is the slope of the liquidus, Γ is the Gibbs-Thomson coefficient, G_c is the solute gradient, G is the thermal gradient and ΔT is the undercooling temperature. Solving equations 13-16 together would give a correlation between the undercooling temperature and the velocity of the dendrite growth.

2.2.3.2 Application of Cellular Automata

CA was developed for casting and has been adapted for welding and laser cladding (Rappaz and Gandin 1993, Zhan, Dong et al. 2008, Yin and Felicelli 2010, Wang, Luo et al. 2014). Wang *et al.* coupled FEM and CA models to predict the grain growth during a single pulse of the laser on Ti6Al4V for laser cladding (Wang, Luo et al. 2014). The model captured the melt pool depth and grain structures for varying laser pulse duration. Dezfoli *et al.* used FEM and CA models to predict the effect of a secondary laser heat source on the microstructure (Dezfoli, Hwang et al. 2017). The model was able to capture the difference in microstructure due to the varying melt pool dimension in 3D. The effects of secondary laser caused the thermal gradient and cooling rate which can cause grains to transit from columnar to equiaxed. Both models did not have the addition of materials that is required in AM but have shown the similarities and can be translated from welding to AM.

CA has been used to simulate the SLM process which was coupled with varying thermal macro models. Zinoviev *et al.* coupled FDM and CA to simulate SLM of 316L, getting the 2D grain structure at the traverse cross section of a melt track for multiple layers (Zinoviev, Zinovieva et al. 2016). Although the model was able to capture the columnar growth, the experiment data displayed small amounts of equiaxed grains and some columnar grains being cut off by another columnar grain. This could be due to the model being only 2D and lack of nucleation that could happen in experiment. Zinoviev *et al.* similarly coupled FDM and CA for 3D grains, however, the grains grew purely columnar which can be different from experimental data which had equiaxed grains (Zinovieva, Zinoviev et al. 2018). This leads to inaccurate grain structure as only columnar grains will grow from bottom to top since no nucleation occurs which differs from experimental data found. Koepf *et al.* simulated in 3D for multiple layers with multiple tracks per layer

for EBM of IN 718 (Koepf, Gotterbarm et al. 2018). The thermal solution was found analytically and CA was used to simulate the grain structure and the simulated grain size and aspect ratio matched the experimental results well through the multiple layers. Similar to the models mentioned above, there are equiaxed grains mixed within the columnar grains which affects the overall grain structure to a certain extent. However, the cause for these equiaxed grains may not be fully understood and can be difficult to capture in the CA models. One issue that multiple tracks and layer CA models must deal with is the large memory required deal to the small cell sizes. Both CA and thermal models would require parallelization and the thermal solution may need to be simplified. Koepf *et al.* used an analytical solution instead of a purely numerical simulation to reduce the computational resource. Koepf et al. used numerical simulation for the thermal model and reused the temperature profile at varying regions in the entire model, rotating by 90 degrees at certain regions (Koepf, Soldner et al. 2019). This reduced the computational memory and storage required for the entire thermal profile. Lopez-Botello *et al.* simulated the microstructure along the longitudinal cross section using 2D FEM and CA models for SLM of AA-2024 (Lopez-Botello, Martinez-Hernandez et al. 2017). The model predicted columnar growth with grain sizes close to experiment data. Nucleation is captured based on experimental data with the probability of nucleation depending on the grain size. Although this method managed to capture the scattered grains, it requires experiments first for tuning of parameters. Rai *et al.* coupled CA with Lattice-Boltzmann to find the microstructure of different laser scanning pattern (Rai, Markl et al. 2016). Although Lattice-Boltzmann method is more accurate than FEM, it is computational resource heavy and difficult to translate to 3D. The grain sizes matched the experimental data that's compared to other literature, however, the grain orientation could not be captured fully as its simulated in 2D and cannot be compared to the EBSD results.

Panwisawas *et al.* coupled CFD and CA models to predict the microstructure of Ti-6Al-4V using SLM (Panwisawas, Qiu et al. 2017). While CFD provides greater detail in terms of melt pool shape and the flow in the melt is accounted for, the volume simulated is limited to a single scan track. This limits the study and single scan tracks may not be able to represent the overall grain structure.

CA has been modified to consider the momentum and species transport equations called modified cellular automata (MCA) (Zhu, Lee et al. 2004). MCA solves the additional equations by finite difference, which is an additional step CA does not have (Wang, Lee et al. 2003). Unlike CA, MCA simulates on the micro-scale also getting the dendrite shape and solute concentration in a given melt pool that is solidifying. MCA have been shown to be able to model for multiple solute elements, CET and also include effects like convection in the melt pool (Zhu, Lee et al. 2004, Michelic, Thuswaldner et al. 2012, Chen, Xu et al. 2014). While having different equations and methods as PFM the results found were similar (Zaeem, Yin et al. 2013). However, MCA have not been applied to AM as of the time of writing.

2.3 Comparison of Microstructure Modelling Methods

A comparison of the length scale and accuracy of the different models is show in **Figure 5**. The smaller the length scale, the smaller the simulation time step needed, this to large amount of data created. Higher accuracy models tend to have more equations and variables to solve which requires more computational resources. In general, accurate models have small length scales, short time step thus limiting in the volume the model can simulate. CFD models tend to only simulate a single melt track while FEM models simulate for multiple melt tracks. PFM models simulate for a few dendrites while CA and MC models simulate the grain structure.

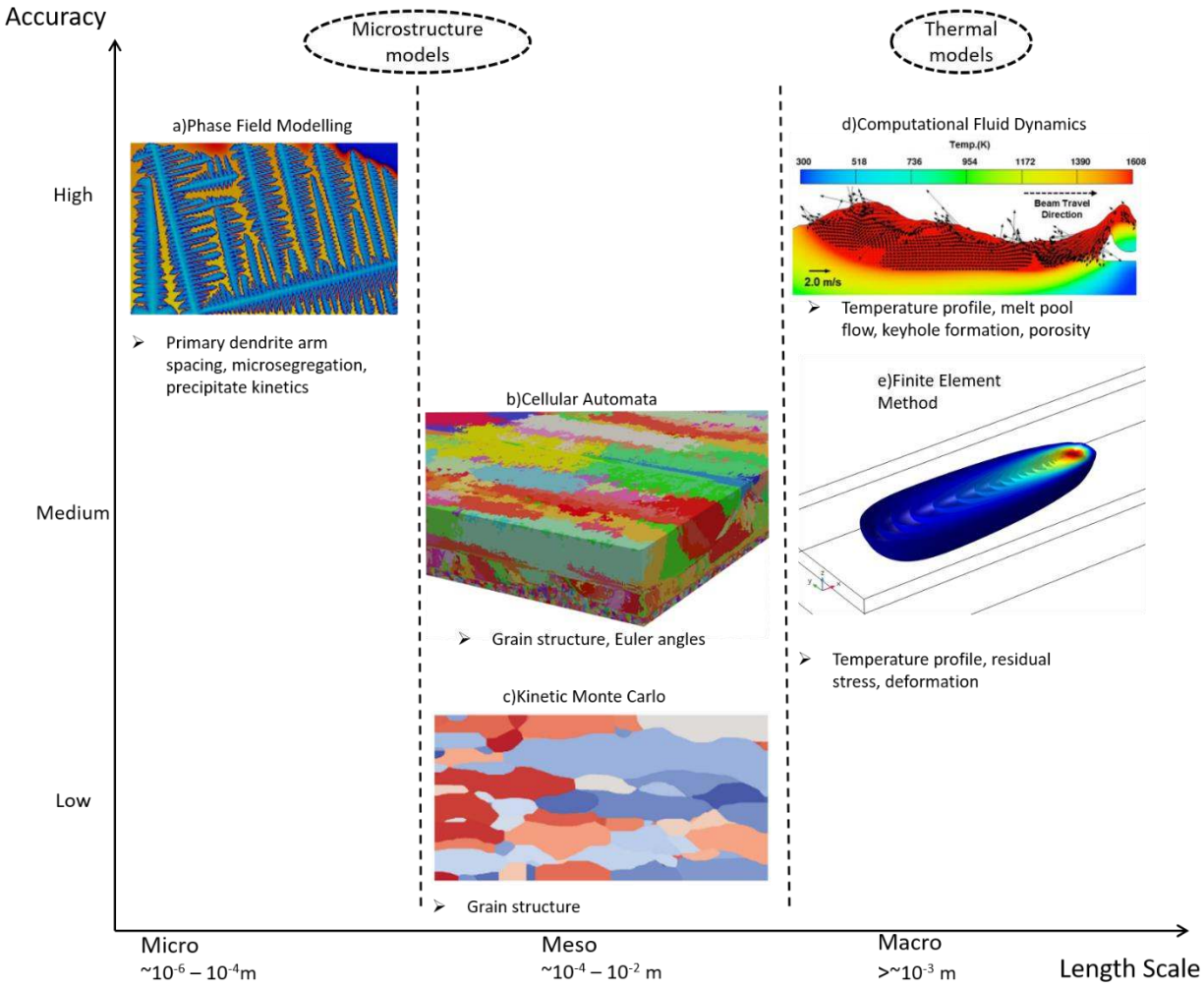

Figure 5. Schematic diagram comparing different models in terms of length scale and accuracy; Representation of each models a)Phase field Modelling, b)Cellular automata, c) kinetic Monte Carlo, "Simulation of metal additive manufacturing microstructures using kinetic Monte Carlo" by T. M. Rodgers *et al.* is licensed under CC BY 4.0 (Rodgers, Madison et al. 2017), d) Computational fluid dynamics, Solid Freeform Fabrication Symposium Proceedings (2015). Copyright 2015 The University of Texas at Austin.(Lee and Zhang 2015) and e) Finite element method.

Comparing the models, PFM not only give realistic dendrite shapes, but it also accounts for the solute distribution between the dendrite arms. When combined with thermodynamic databases, TTT and CTT curves, PFM can have not only very accurate details of solute distribution and dendrite shapes and sizes but also predict the composition of the various metals and intermetallic and transformation and growth of precipitates (Ferreira, Paradela et al. 2017, Mullis, Bollada et al. 2018, Böttger, Apel et al. 2019). All the PFM models for AM were in 2D and only simulated for a few dendrites.

This is most likely being due to the computational resources required thus making 3D models time-consuming and expensive to run. MCA have been modelled in 3D and have been shown to be more efficient and faster than PFM while having the similar results, however, simulations are also done on small number of dendrites (Wang, Lee et al. 2003, Zaeem, Yin et al. 2013).

MC and CA models forgo details like solute concentration and dendrite shape and instead simulate grain structures. Both models provide information like the grain width and aspect ratio. One difference is CA models accounts for the preferred crystallographic growth direction of metals. As the direction and speed the crystal grows is dependent on the preferred direction and direction of the thermal gradient, MC may not get accurate grain size and aspect ratio. CA uses solidification theory to calculate the solidification speed of the preferential dendrite crystallographic direction. This leads to CA models being more accurate than MC models. CA has been modelled in both 2D and 3D. A comparison of all the models is shown in **Table 1**.

Table 1. Comparison of microstructure models

Simulation method	Phase Field Method	Modified Cellular Automata	Kinetic Monte Carlo	Cellular Automata
Computational resource	High	High	Low	Moderate
Length scale	0.025-0.2 µm <100x100 µm^2 ~200k to 1M cells	0.3-0.4 µm <100x100 µm^2 ~1M cells	1-10 µm <2x2x2 mm^3 ~1-50M sites	1-10 µm <2x2x2 mm^3 ~1-50M cells
Mesh shape	Square	Square/hexagon	Points	Square/hexagon
Experiments required	Few, for validation	Few, for validation	Several, for tuning & validation	Few, for tuning & validation
Level of details	Dendrite shape Dendrite angle	Dendrite shape Dendrite angle	Grain size Grain shape	Grain size Grain shape

	Solute concentration & precipitates Grain size Grain shape	Solute concentration		Dendrite angle
Probabilistic/ Deterministic	✓ Deterministic ✓ Probabilistic	✓ Deterministic ✓ Probabilistic	✓ Probabilistic	✓ Deterministic ✓ Probabilistic
Commercial software	Yes	No	No	No
Open source software	Yes	No	Yes	Limited
References	(Cao and Choi 2006, Farzadi, Do-Quang et al. 2008, Fallah, Amoorezaei et al. 2012, Montiel, Liu et al. 2012, Sahoo and Chou 2014, Gong and Chou 2015, Sahoo and Chou 2016, Acharya, Sharon et al. 2017, Keller, Lindwall et al. 2017, Kumara, Deng et al. 2019, Kumara, Segerstark et al. 2019)	(Wang, Lee et al. 2003, Zhu, Lee et al. 2004, Michelic, Thuswaldner et al. 2012, Zaeem, Yin et al. 2013, Chen, Xu et al. 2014)	(Yang, Sista et al. 2000, Mishra and DebRoy 2004, Mishra and DebRoy 2004, Zhong 2011, Liu, Cheng et al. 2014, Wang, Liu et al. 2014, Rodgers, Madison et al. 2016, Rodgers, Madison et al. 2017, Wei, Elmer et al. 2017)	(Yin and Felicelli 2010, Zaeem, Yin et al. 2013, Wang, Luo et al. 2014, Rai, Markl et al. 2016, Zhou, Zhang et al. 2016, Zinoviev, Zinovieva et al. 2016, Dezfoli, Hwang et al. 2017, Lopez-Botello, Martinez-Hernandez et al. 2017, Panwisawas, Qiu et al. 2017)

3 Potential and Challenges of Microstructure Modelling in AM

Modelling for microstructure require thermal models as they provide the temperature, cooling rate and temperature gradient for inputs to the microstructure model. Having more accurate cooling rates and temperature gradients can lead to better predictability of microstructure. However, the length scale of the models is either for a single track scan or for multiple tracks and multiple layers, with CFD being used most often to simulate

for a single line and FEM for multiple tracks and layers. This most likely happen due to the computational resource limitation. FEM models have to use bulk material properties and for the powder bed, the porosity of the powder bed is used to estimate the bulk properties. However, finding the porosity of the powder bed is difficult, the density of a powder bed can be estimated to the apparent density. The apparent density can be found using a Scott volumeter, but during the recoating of the powder during a PBF process the underlying surface is uneven and actual distribution of powder is unknown, this will cause the density of the powder bed to vary. FEM models have codes developed to allow mesh refining and coarsening or having lumped heat per layer to reduce computational time and increase the volume simulated (Papadakis, Loizou et al. 2014, Patil, Pal et al. 2015). However, the FEM codes were written to help improve simulation time for AM processes and commercial FEM software are currently unable to reproduce it at the time of writing. CFD models on the other hand are not replicating the volume FEM models are making but instead focus on the different phenomena in the melt pool. This tends to have more accurate melt pool geometries, cooling rate and temperature gradient. The shape of the tracks is closer to experimental results. However, all these are done for a single or few tracks that is usually much smaller than actual print size. The more accurate the details are, the better it is for the microstructure model as better growth kinetics can be predicted. A challenge thermal model face in getting accurate temperature is an accurate input of the heat source. FEM models tend to take a heat distribution either as a 2D input on the top surface or as a 3D volumetric heat (Loh, Chua et al. 2015, Yin, Peng et al. 2018). This heat input often uses estimated power and absorptivity. CFD models can use ray tracing to model for laser PBF which leads to higher accuracy (King, Anderson et al. 2015). However, in all models, the emissivity and absorptivity can change with temperature and this is difficult to capture in experiments.

Thermal models are considered macro scale in comparison with microstructure models which are micro or meso scale. MC and CA both are better suited to simulate for large volumes as they require lesser calculations while PFM and MCA require more calculations and simulates for a smaller volume. The choice of models to use comes down to the length scale required. Apart from the length scale, each microstructure models also face challenges.

The dendrite shape and solute concentration that micro-scale models predict can be used to investigate new materials to be used in AM. Having an estimate on element phases and solute concentration can help in knowing if defects like hot cracking are likely to form or segregation of alloying elements (Keller, Lindwall et al. 2017, Gao, Agarwal et al. 2018). However, PFM and MCA also face certain challenges. Both models currently only model the solidification portion without the melting portion. Instead, seeds are placed in predefined positions. While this may provide an estimate of the PDAS, the actual size of the dendrite is dependent on the given spacing from each seed. This leads to bias based on the seed position placed and changing of material or process parameters may require changes in seeds positioning or experiments to provide better positioning. Another challenge is the computational resources required in micro-scale modelling (Glicksman 2010). This limits the volume of the simulation to within a single grain or a few grains. PFM models reviewed in this paper reduced the alloy to a binary alloy thus only finding the solute concentration or precipitate of a single solute. Microsegregation occurs in as-built AM parts and causes non-homogenous microstructure (Ghosh 2018). Simulating for multicomponent alloy could help in studying how segregation occurs and possible work arounds, however, it would increase computational time as the equations would have to solve the summations of each components (Nestler, Garcke et al. 2005). MC models do not face this issue as it does not account for solutes. CA models uses solidification theory

which can account for multiple elements, however, most model also reduces it to binary or tertiary alloys (Zineviva, Columnar to equiaxed transition during alloy solidification). Due to the nature of AM, depending on the scanning strategy, tracks can be re-melted several times. For PBF processes, tracks are often overlapping causing a single track to be melted at the sides and the next layer would also cause the top portion of previous layer to melt. The grain structure of the metal would then depend on the melting and growing of grains from previously printed tracks. In order to track the grain structure, microstructure models would have to be able to simulate a large enough volume to investigate different scanning strategies. In this aspect meso-scale MC and CA models would work well as it has been shown to be able to model in 3D as well as for multiple tracks and layers. A challenge for MC models is to get results closer to experimental data, although the trends of the grain structure is captured, the aspect ratio differs (Rodgers, Madison et al. 2017, Sun, Tan et al. 2018). CA models faces challenges in getting the scattered mix of equiaxed grains found in experimental data (Rai, Markl et al. 2016, Zinoviev, Zinovieva et al. 2016, Zinovieva, Zinoviev et al. 2018). Most CA models depend on nucleation models used in casting or do not implement nucleation, similar to welding CA models. This leads to grains that grow indefinitely in the build direction which differs from experimental data. Botello *et al.* CA model managed to capture similar grain aspect ratio but relies on experimental data to enable nucleation. This requires experiments on new material and process parameters to accurately model it. New nucleation methods may have to be used to capture nucleation in CA models.

Meshing plays an important role in numerical models and inappropriate meshing can lead to inaccurate results or alter results causing mesh anisotropy. PFM models have very thin interface which requires very small cell sizes at the interface, however, the small cell size also reduces the time step of the model creating large amounts of data and requires more

computational time for the same amount of time length (Zhang, Li et al. 2019). Some models use adaptive meshing to reduce the number of total cells (Francois, Sun et al. 2017). Kinetic MC and CA also face the similar problem of having smaller cell sizes requiring small time steps leading to large amounts of data and computational resource. CA also can face mesh anisotropy and to counter this some models use hexagonal cells, however, majority of the models use the decentred square method developed by Gandin and Rappaz which allows square cells while eliminating mesh anisotropy (Gandin and Rappaz 1997, Dezfoli, Hwang et al. 2017, Panwisawas, Qiu et al. 2017).

4 Conclusion

Numerical modelling can help in predicting microstructure without the need of experiments. The grain structure, microsegregation, precipitate and dendrite size can be predicted using varying microstructure models. In order to get it two models are usually coupled together, thermal model and microstructure model. Two types of thermal models and three types of microstructure modelling for AM are reviewed. The macro thermal models predict the temperature, cooling rate and temperature gradient which is used as input for microstructure models.

Of the two types of thermal models, FEM is most often used to model for multiple tracks and layers, while CFD is used for simulating for limited number of tracks. FEM models ignore the flow of the fluid reducing the amount of computation required and thus are able to simulate a larger volume. CFD models often focus on the physics of the melt pool, requiring more computation resources. FEM models being able to simulate larger volumes can be used in microstructure modelling to simulate the grain structure where grains often grow over multiple layers. CFD models has more accurate cooling rate and temperature gradient can be used to get more accurate microstructure.

There are two different scales that microstructure modelling can take place: micro-scale and meso-scale. Micro-scale models simulate the dendrites and the solute composition while meso-scale simulates the grain structures. PFM and MCA are able to simulate on the micro-scale getting the segregation of alloying elements and finding the PDAS which relates to the local strength and hardness. It however requires large computational resource limiting its volume to simulate for a few dendrites. MC and CA are able to simulate a larger volume getting the grain structure. The grain size and aspect ratio which relates to the strength and ductility of the part is found in both models. MC models, however, have poorer prediction in grain size as compared to CA models. PFM and MCA can be useful in finding how new materials would form in the AM process and can facilitate the addition of new materials for AM. The overall mechanical properties would also depend on the size and aspect ratio of grain structure which would require MC or CA to model. Depending on the type of mechanical properties to be predicted, simulation has to be done in different length scales.

Acknowledgement

This research is supported by the National Research Foundation, Prime Minister's Office, Singapore under its Medium-Sized Centre funding scheme.

References

Acharya, R., J. A. Sharon and A. Staroselsky (2017). "Prediction of microstructure in laser powder bed fusion process." Acta Materialia **124**: 360-371.

Amato, K., J. Hernandez, L. Murr, E. Martinez, S. Gaytan, P. Shindo and S. Collins (2012). "Comparison of microstructures and properties for a Ni-base superalloy (Alloy 625) fabricated by electron and laser beam melting." Journal of Materials Science Research **1**(2): 3.

Andani, M. T., R. Dehghani, M. R. Karamooz-Ravari, R. Mirzaeifar and J. Ni (2017). "A Study on the Effect of Energy Input on Spatter Particles Creation during Selective Laser Melting Process." Additive Manufacturing.

Atzeni, E. and A. Salmi (2012). "Economics of additive manufacturing for end-usable metal parts." The International Journal of Advanced Manufacturing Technology **62**(9): 1147-1155.

Baufeld, B., O. Van der Biest and R. Gault (2010). "Additive manufacturing of Ti-6Al-4V components by shaped metal deposition: Microstructure and mechanical properties." Materials & Design **31**: S106-S111.

Boettinger, W. J., J. A. Warren, C. Beckermann and A. Karma (2002). "Phase-field simulation of solidification." Annual review of materials research **32**(1): 163-194.
Böttger, B., M. Apel, B. Daniels, L. Dankl, T. Göhler and T. Jokisch (2019). "Systematic Phase-Field Study on Microstructure Formation During Brazing of Mar-M247 with a Si-Based AMS4782 Filler." Metallurgical and Materials Transactions A **50**(4): 1732-1747.
Brunette, D. M., P. Tengvall, M. Textor and P. Thomsen (2012). Titanium in medicine: material science, surface science, engineering, biological responses and medical applications, Springer Science & Business Media.
Cantor, B., H. Assender and P. Grant (2015). Aerospace materials, CRC Press.
Cao, Y. and J. Choi (2006). "Multiscale modeling of solidification during laser cladding process." Journal of Laser Applications **18**(3): 245-257.
Chen, L.-Q. (2002). "Phase-field models for microstructure evolution." Annual review of materials research **32**(1): 113-140.
Chen, R., Q. Xu and B. Liu (2014). "A modified cellular automaton model for the quantitative prediction of equiaxed and columnar dendritic growth." Journal of Materials Science & Technology **30**(12): 1311-1320.
Chen, S., G. Guillemot and C.-A. Gandin (2016). "Three-dimensional cellular automaton-finite element modeling of solidification grain structures for arc-welding processes." Acta Materialia **115**: 448-467.
Chiumenti, M., E. Neiva, E. Salsi, M. Cervera, S. Badia, J. Moya, Z. Chen, C. Lee and C. Davies (2017). "Numerical modelling and experimental validation in selective laser melting." Additive Manufacturing **18**: 171-185.
Chua, C. K. and K. F. Leong (2017). 3D Printing and Additive Manufacturing - Principles and Applications World Scientific Publishing Co. Pte Ltd.
Clijsters, S., T. Craeghs, S. Buls, K. Kempen and J. P. Kruth (2014). "In situ quality control of the selective laser melting process using a high-speed, real-time melt pool monitoring system." International Journal of Advanced Manufacturing Technology **75**(5-8): 1089-1101.
Degenhardt, R. (2017). Advanced Lattice Boltzmann Models for the Simulation of Additive Manufacturing Processes.
Dehoff, R., M. Kirka, W. Sames, H. Bilheux, A. Tremsin, L. Lowe and S. Babu (2015). "Site specific control of crystallographic grain orientation through electron beam additive manufacturing." Materials Science and Technology **31**(8): 931-938.
Denlinger, E. R. (2018). Development and Numerical Verification of a Dynamic Adaptive Mesh Coarsening Strategy for Simulating Laser Power Bed Fusion Processes. Thermo-Mechanical Modeling of Additive Manufacturing, Elsevier**:** 199-213.
Denlinger, E. R., J. C. Heigel and P. Michaleris (2015). "Residual stress and distortion modeling of electron beam direct manufacturing Ti-6Al-4V." Proceedings of the Institution of Mechanical Engineers, Part B: Journal of Engineering Manufacture **229**(10): 1803-1813.
Dezfoli, A. R. A., W.-S. Hwang, W.-C. Huang and T.-W. Tsai (2017). "Determination and controlling of grain structure of metals after laser incidence: Theoretical approach." Scientific Reports **7**: 41527.
Elder, K., M. Grant, N. Provatas and J. Kosterlitz (2001). "Sharp interface limits of phase-field models." Physical Review E **64**(2): 021604.
Everton, S. K., M. Hirsch, P. Stravroulakis, R. K. Leach and A. T. Clare (2016). "Review of in-situ process monitoring and in-situ metrology for metal additive manufacturing." Materials & Design **95**: 431-445.
Fallah, V., M. Alimardani, S. F. Corbin and A. Khajepour (2011). "Temporal development of melt-pool morphology and clad geometry in laser powder deposition." Computational materials science **50**(7): 2124-2134.
Fallah, V., M. Amoorezaei, N. Provatas, S. Corbin and A. Khajepour (2012). "Phase-field simulation of solidification morphology in laser powder deposition of Ti–Nb alloys." Acta Materialia **60**(4): 1633-1646.

Farzadi, A., M. Do-Quang, S. Serajzadeh, A. Kokabi and G. Amberg (2008). "Phase-field simulation of weld solidification microstructure in an Al–Cu alloy." Modelling and Simulation in Materials Science and Engineering **16**(6): 065005.
Ferreira, A. F., K. G. Paradela, P. Felipe Junior, Z. Alcântara Júnior and A. Garcia (2017). "Phase-Field Simulation of Microsegregation and Dendritic Growth During Solidification of Hypoeutectic Al-Cu alloys." Materials Research **20**(2): 423-429.
Foroozmehr, A., M. Badrossamay, E. Foroozmehr and S. Golabi (2016). "Finite Element Simulation of Selective Laser Melting process considering Optical Penetration Depth of laser in powder bed." Materials & Design **89**: 255-263.
Francois, M. M., A. Sun, W. E. King, N. J. Henson, D. Tourret, C. A. Bronkhorst, N. N. Carlson, C. K. Newman, T. Haut and J. Bakosi (2017). "Modeling of additive manufacturing processes for metals: Challenges and opportunities." Current Opinion in Solid State and Materials Science.
Frazier, W. E. (2014). "Metal additive manufacturing: a review." Journal of Materials Engineering and Performance **23**(6): 1917-1928.
Gandin, C.-A., J.-L. Desbiolles, M. Rappaz and P. Thevoz (1999). "A three-dimensional cellular automation-finite element model for the prediction of solidification grain structures." Metallurgical and Materials Transactions A **30**(12): 3153-3165.
Gandin, C.-A. and M. Rappaz (1994). "A coupled finite element-cellular automaton model for the prediction of dendritic grain structures in solidification processes." Acta metallurgica et materialia **42**(7): 2233-2246.
Gandin, C.-A. and M. Rappaz (1997). "A 3D cellular automaton algorithm for the prediction of dendritic grain growth." Acta Materialia **45**(5): 2187-2195.
Gao, H., G. Agarwal, M. Amirthalingam and M. Hermans (2018). "Hot cracking investigation during laser welding of high-strength steels with multi-scale modelling approach." Science and Technology of Welding and Joining **23**(4): 287-294.
Ghosh, S. (2018). "Predictive modeling of solidification during laser additive manufacturing of nickel superalloys: recent developments, future directions." Materials Research Express **5**(1): 012001.
Gibson, I., D. W. Rosen and B. Stucker (2010). Additive manufacturing technologies, Springer.
Gifkins, R. C. (1976). "Grain-boundary sliding and its accommodation during creep and superplasticity." Metallurgical and Materials Transactions A **7**(8): 1225-1232.
Glicksman, M. E. (2010). Principles of solidification: an introduction to modern casting and crystal growth concepts, Springer Science & Business Media.
Gong, X. and K. Chou (2015). "Phase-field modeling of microstructure evolution in electron beam additive manufacturing." JOM **67**(5): 1176-1182.
Gránásy, L., T. Pusztai and J. A. Warren (2004). "Modelling polycrystalline solidification using phase field theory." Journal of Physics: Condensed Matter **16**(41): R1205.
Guo, P., B. Zou, C. Huang and H. Gao (2017). "Study on microstructure, mechanical properties and machinability of efficiently additive manufactured AISI 316L stainless steel by high-power direct laser deposition." Journal of Materials Processing Technology **240**: 12-22.
Gürtler, F., M. Karg, K. Leitz and M. Schmidt (2013). "Simulation of laser beam melting of steel powders using the three-dimensional volume of fluid method." Physics Procedia **41**(1): 874-879.
Huang, Y., M. C. Leu, J. Mazumder and A. Donmez (2015). "Additive Manufacturing: Current State, Future Potential, Gaps and Needs, and Recommendations." Journal of Manufacturing Science and Engineering-Transactions of the Asme **137**(1).
Keller, T., G. Lindwall, S. Ghosh, L. Ma, B. M. Lane, F. Zhang, U. R. Kattner, E. A. Lass, J. C. Heigel and Y. Idell (2017). "Application of finite element, phase-field, and calphad-based methods to additive manufacturing of Ni-based superalloys." Acta Materialia **139**: 244-253.
Khairallah, S. A., A. T. Anderson, A. Rubenchik and W. E. King (2016). "Laser powder-bed fusion additive manufacturing: Physics of complex melt flow and formation mechanisms of pores, spatter, and denudation zones." Acta Materialia **108**: 36-45.

Kim, S. G. and W. T. Kim (2005). "Phase-Field Modeling of Solidification." Handbook of Materials Modeling: 2105-2116.
King, W. E., A. T. Anderson, R. Ferencz, N. Hodge, C. Kamath, S. A. Khairallah and A. M. Rubenchik (2015). "Laser powder bed fusion additive manufacturing of metals; physics, computational, and materials challenges." Applied Physics Reviews **2**(4): 041304.
Koepf, J., D. Soldner, M. Ramsperger, J. Mergheim, M. Markl and C. Körner (2019). "Numerical microstructure prediction by a coupled finite element cellular automaton model for selective electron beam melting." Computational Materials Science **162**: 148-155.
Koepf, J. A., M. R. Gotterbarm, M. Markl and C. Körner (2018). "3D multi-layer grain structure simulation of powder bed fusion additive manufacturing." Acta Materialia **152**: 119-126.
Körner, C., A. Bauereiß and E. Attar (2013). "Fundamental consolidation mechanisms during selective beam melting of powders." Modelling and Simulation in Materials Science and Engineering **21**(8): 085011.
Körner, C., H. Helmer, A. Bauereiß and R. F. Singer (2014). Tailoring the grain structure of IN718 during selective electron beam melting. MATEC Web of Conferences, EDP Sciences.
Kou, S. (2003). Welding metallurgy, John Wiley & Sons.
Kumara, C., D. Deng, F. Hanning, M. Raanes, J. Moverare and P. Nylén (2019). "Predicting the Microstructural Evolution of Electron Beam Melting of Alloy 718 with Phase-Field Modeling." Metallurgical and Materials Transactions A **50**(5): 2527-2537.
Kumara, C., A. Segerstark, F. Hanning, N. Dixit, S. Joshi, J. Moverare and P. Nylén (2019). "Microstructure modelling of laser metal powder directed energy deposition of alloy 718." Additive Manufacturing **25**: 357-364.
Kurz, W., B. Giovanola and R. Trivedi (1986). "Theory of microstructural development during rapid solidification." Acta metallurgica **34**(5): 823-830.
Lee, Y. and W. Zhang (2015). Mesoscopic simulation of heat transfer and fluid flow in laser powder bed additive manufacturing. Proceedings of the Annual International Solid Freeform Fabrication Symposium, Austin, TX, USA.
Lee, Y. and W. Zhang (2015). Mesoscopic simulation of heat transfer and fluid flow in laser powder bed additive manufacturing. International Solid Free Form Fabrication Symposium, Austin.
Lewandowski, J. J. and M. Seifi (2016). "Metal additive manufacturing: a review of mechanical properties." Annual Review of Materials Research **46**: 151-186.
Lindgren, L.-E., H.-A. Häggblad, J. McDill and A. S. Oddy (1997). "Automatic remeshing for three-dimensional finite element simulation of welding." Computer Methods in Applied Mechanics and Engineering **147**(3-4): 401-409.
Liu, D. and Y. Wang (2017). Mesoscale Multi-Physics Simulation of Solidification in Selective Laser Melting Process Using a Phase Field and Thermal Lattice Boltzmann Model. ASME 2017 International Design Engineering Technical Conferences and Computers and Information in Engineering Conference, American Society of Mechanical Engineers.
Liu, S., H. Zhu, G. Peng, J. Yin and X. Zeng (2018). "Microstructure prediction of selective laser melting AlSi10Mg using finite element analysis." Materials & Design **142**: 319-328.
Liu, Y., L. Cheng, Q. Zeng, Z. Feng, J. Zhang, J. Peng, C. Xie and K. Guan (2014). "Monte Carlo simulation of polycrystalline microstructures and finite element stress analysis." Materials & Design **55**: 740-746.
Loh, L.-E., C.-K. Chua, W.-Y. Yeong, J. Song, M. Mapar, S.-L. Sing, Z.-H. Liu and D.-Q. Zhang (2015). "Numerical investigation and an effective modelling on the Selective Laser Melting (SLM) process with aluminium alloy 6061." International Journal of Heat and Mass Transfer **80**: 288-300.
Lopez-Botello, O., U. Martinez-Hernandez, J. Ramírez, C. Pinna and K. Mumtaz (2017). "Two-dimensional simulation of grain structure growth within selective laser melted AA-2024." Materials & Design **113**: 369-376.

Lu, J., K. Luo, Y. Zhang, G. Sun, Y. Gu, J. Zhou, X. Ren, X. Zhang, L. Zhang and K. Chen (2010). "Grain refinement mechanism of multiple laser shock processing impacts on ANSI 304 stainless steel." Acta Materialia **58**(16): 5354-5362.
Lu, Q. Y. and C. H. Wong (2018). "Additive manufacturing process monitoring and control by non-destructive testing techniques: challenges and in-process monitoring." Virtual and Physical Prototyping **13**(2): 39-48.
Mercelis, P. and J.-P. Kruth (2006). "Residual stresses in selective laser sintering and selective laser melting." Rapid Prototyping Journal **12**(5): 254-265.
Michelic, S., J. Thuswaldner and C. Bernhard (2012). A modified cellular automaton method for polydimensional modelling of dendritic growth and microsegregation in multicomponent alloys. IOP Conference Series: Materials Science and Engineering, IOP Publishing.
Mishra, S. and T. DebRoy (2004). "Grain topology in Ti–6Al–4V welds—Monte Carlo simulation and experiments." Journal of Physics D: Applied Physics **37**(15): 2191.
Mishra, S. and T. DebRoy (2004). "Measurements and Monte Carlo simulation of grain growth in the heat-affected zone of Ti–6Al–4V welds." Acta Materialia **52**(5): 1183-1192.
Miyoshi, E., T. Takaki, M. Ohno, Y. Shibuta, S. Sakane and T. Aoki (2019). "Large-scale phase-field simulation of three-dimensional isotropic grain growth in polycrystalline thin films." Modelling and Simulation in Materials Science and Engineering **27**(5): 054003.
Montiel, D., L. Liu, L. Xiao, Y. Zhou and N. Provatas (2012). "Microstructure analysis of AZ31 magnesium alloy welds using phase-field models." Acta Materialia **60**(16): 5925-5932.
Mullis, A. M., P. C. Bollada and P. K. Jimack (2018). Phase-Field Modelling of Intermetallic Solidification. TMS Annual Meeting & Exhibition, Springer.
Murr, L. E., S. M. Gaytan, D. A. Ramirez, E. Martinez, J. Hernandez, K. N. Amato, P. W. Shindo, F. R. Medina and R. B. Wicker (2012). "Metal fabrication by additive manufacturing using laser and electron beam melting technologies." Journal of Materials Science & Technology **28**(1): 1-14.
Nestler, B., H. Garcke and B. Stinner (2005). "Multicomponent alloy solidification: phase-field modeling and simulations." Physical Review E **71**(4): 041609.
Nie, P., O. Ojo and Z. Li (2014). "Numerical modeling of microstructure evolution during laser additive manufacturing of a nickel-based superalloy." Acta Materialia **77**: 85-95.
Panwisawas, C., C. Qiu, M. J. Anderson, Y. Sovani, R. P. Turner, M. M. Attallah, J. W. Brooks and H. C. Basoalto (2017). "Mesoscale modelling of selective laser melting: Thermal fluid dynamics and microstructural evolution." Computational Materials Science **126**: 479-490.
Papadakis, L., A. Loizou, J. Risse, S. Bremen and J. Schrage (2014). "A computational reduction model for appraising structural effects in selective laser melting manufacturing: a methodical model reduction proposed for time-efficient finite element analysis of larger components in Selective Laser Melting." Virtual and Physical Prototyping **9**(1): 17-25.
Parimi, L. L., G. Ravi, D. Clark and M. M. Attallah (2014). "Microstructural and texture development in direct laser fabricated IN718." Materials Characterization **89**: 102-111.
Patil, N., D. Pal, H. K. Rafi, K. Zeng, A. Moreland, A. Hicks, D. Beeler and B. Stucker (2015). "A Generalized Feed Forward Dynamic Adaptive Mesh Refinement and Derefinement Finite Element Framework for Metal Laser Sintering—Part I: Formulation and Algorithm Development." Journal of Manufacturing Science and Engineering **137**(4): 041001.
Peel, M., A. Steuwer, M. Preuss and P. Withers (2003). "Microstructure, mechanical properties and residual stresses as a function of welding speed in aluminium AA5083 friction stir welds." Acta materialia **51**(16): 4791-4801.
Pinkerton, A. J. (2015). "Advances in the modeling of laser direct metal deposition." Journal of laser applications **27**(S1): S15001.
Raghavan, N., R. Dehoff, S. Pannala, S. Simunovic, M. Kirka, J. Turner, N. Carlson and S. S. Babu (2016). "Numerical modeling of heat-transfer and the influence of process parameters on tailoring the grain morphology of IN718 in electron beam additive manufacturing." Acta Materialia **112**: 303-314.

Rai, A., M. Markl and C. Körner (2016). "A coupled Cellular Automaton–Lattice Boltzmann model for grain structure simulation during additive manufacturing." Computational Materials Science **124**: 37-48.
Rappaz, M. and C.-A. Gandin (1993). "Probabilistic modelling of microstructure formation in solidification processes." Acta metallurgica et materialia **41**(2): 345-360.
Rausch, A. M., V. E. Küng, C. Pobel, M. Markl and C. Körner (2017). "Predictive Simulation of Process Windows for Powder Bed Fusion Additive Manufacturing: Influence of the Powder Bulk Density." Materials **10**(10): 1117.
Rodgers, T. M., J. D. Madison and V. Tikare (2017). "Simulation of metal additive manufacturing microstructures using kinetic Monte Carlo." Computational Materials Science **135**: 78-89.
Rodgers, T. M., J. D. Madison, V. Tikare and M. C. Maguire (2016). "Predicting mesoscale microstructural evolution in electron beam welding." JOM **68**(5): 1419-1426.
Roehling, T. T., S. S. Wu, S. A. Khairallah, J. D. Roehling, S. S. Soezeri, M. F. Crumb and M. J. Matthews (2017). "Modulating laser intensity profile ellipticity for microstructural control during metal additive manufacturing." Acta Materialia **128**: 197-206.
Rolchigo, M. R., M. Y. Mendoza, P. Samimi, D. A. Brice, B. Martin, P. C. Collins and R. LeSar (2017). "Modeling of Ti-W solidification microstructures under additive manufacturing conditions." Metallurgical and Materials Transactions A **48**(7): 3606-3622.
Sahoo, S. and K. Chou (2014). Review on phase-field modeling of microstructure evolutions: application to electron beam additive manufacturing. ASME 2014 International manufacturing science and engineering conference, MSEC 2014 collocated with the JSME 2014 international conference on materials and processing and the 42nd North American manufacturing research conference.
Sahoo, S. and K. Chou (2016). "Phase-field simulation of microstructure evolution of Ti–6Al–4V in electron beam additive manufacturing process." Additive manufacturing **9**: 14-24.
Seufzer, W. J. (2014). Additive Manufacturing Modeling and Simulation A Literature Review for Electron Beam Free Form Fabrication.
Shuai, C., L. Xue, C. Gao, Y. Yang, S. Peng and Y. Zhang (2018). "Selective laser melting of Zn–Ag alloys for bone repair: microstructure, mechanical properties and degradation behaviour." Virtual and Physical Prototyping: 1-9.
Singer-Loginova, I. and H. Singer (2008). "The phase field technique for modeling multiphase materials." Reports on progress in physics **71**(10): 106501.
Stefanescu, D. (2015). Science and engineering of casting solidification, Springer.
Steinbach, I. (2009). "Phase-field models in materials science." Modelling and simulation in materials science and engineering **17**(7): 073001.
Sun, Z., X. Tan, S. B. Tor and C. K. Chua (2018). "Simultaneously enhanced strength and ductility for 3D-printed stainless steel 316L by selective laser melting." NPG Asia Materials: 1.
Tan, X., Y. Kok, Y. J. Tan, M. Descoins, D. Mangelinck, S. B. Tor, K. F. Leong and C. K. Chua (2015). "Graded microstructure and mechanical properties of additive manufactured Ti–6Al–4V via electron beam melting." Acta Materialia **97**: 1-16.
Vandenbroucke, B. and J.-P. Kruth (2007). "Selective laser melting of biocompatible metals for rapid manufacturing of medical parts." Rapid Prototyping Journal **13**(4): 196-203.
Vastola, G., Q. X. Pei and Y. W. Zhang "Predictive model for porosity in powder-bed fusion additive manufacturing at high beam energy regime." Additive Manufacturing.
Wang, R., Y. Liu and D. Q. Wei (2014). Microstructures in solidification simulation of electron beam scanning with MC in molten pool. Advanced Materials Research, Trans Tech Publ.
Wang, W., P. D. Lee and M. Mclean (2003). "A model of solidification microstructures in nickel-based superalloys: predicting primary dendrite spacing selection." Acta materialia **51**(10): 2971-2987.
Wang, Z.-j., S. Luo, H.-w. Song, W.-d. Deng and W.-y. Li (2014). "Simulation of microstructure during laser rapid forming solidification based on cellular automaton." Mathematical Problems in Engineering **2014**.

Warren, J. A. and W. J. Boettinger (1995). "Prediction of dendritic growth and microsegregation patterns in a binary alloy using the phase-field method." Acta Metallurgica et Materialia **43**(2): 689-703.
Wei, H., J. Elmer and T. DebRoy (2017). "Three-dimensional modeling of grain structure evolution during welding of an aluminum alloy." Acta Materialia **126**: 413-425.
Wei, H., J. Mazumder and T. DebRoy (2015). "Evolution of solidification texture during additive manufacturing." Scientific reports **5**.
Yang, Y., M. Jamshidinia, P. Boulware and S. Kelly (2018). "Prediction of microstructure, residual stress, and deformation in laser powder bed fusion process." Computational Mechanics **61**(5): 599-615.
Yang, Z., S. Sista, J. Elmer and T. DebRoy (2000). "Three dimensional Monte Carlo simulation of grain growth during GTA welding of titanium." Acta Materialia **48**(20): 4813-4825.
Yin, H. and S. Felicelli (2010). "Dendrite growth simulation during solidification in the LENS process." Acta Materialia **58**(4): 1455-1465.
Yin, J., G. Peng, C. Chen, J. Yang, H. Zhu, L. Ke, Z. Wang, D. Wang, M. Ma and G. Wang (2018). "Thermal behavior and grain growth orientation during selective laser melting of Ti-6Al-4V alloy." Journal of Materials Processing Technology **260**: 57-65.
Yuan, P. and D. Gu (2015). "Molten pool behaviour and its physical mechanism during selective laser melting of TiC/AlSi10Mg nanocomposites: simulation and experiments." Journal of Physics D: Applied Physics **48**(3): 035303.
Zaeem, M. A., H. Yin and S. D. Felicelli (2013). "Modeling dendritic solidification of Al–3% Cu using cellular automaton and phase-field methods." Applied Mathematical Modelling **37**(5): 3495-3503.
Zeng, K., D. Pal, H. Gong, N. Patil and B. Stucker (2015). "Comparison of 3DSIM thermal modelling of selective laser melting using new dynamic meshing method to ANSYS." Materials Science and Technology **31**(8): 945-956.
Zhan, X., Z. Dong, Y. Wei and Y. Xu (2008). "Dendritic grain growth simulation in weld molten pool based on CA-FD model." Crystal Research and Technology **43**(3): 253-259.
Zhang, J., X. Li, D. Xu and R. Yang (2019). "Recent progress in the simulation of microstructure evolution in titanium alloys." Progress in Natural Science: Materials International.
Zhong, F. (2011). Applications of Monte Carlo method in science and engineering, InTech.
Zhou, X., H. Zhang, G. Wang, X. Bai, Y. Fu and J. Zhao (2016). "Simulation of microstructure evolution during hybrid deposition and micro-rolling process." Journal of materials science **51**(14): 6735-6749.
Zhu, M., S. Lee and C. Hong (2004). "Modified cellular automaton model for the prediction of dendritic growth with melt convection." Physical Review E **69**(6): 061610.
Zielinski, J., S. Vervoort, H.-W. Mindt and M. Megahed (2017). "Influence of powder bed characteristics on material quality in additive manufacturing." BHM Berg-und Hüttenmännische Monatshefte **162**(5): 192-198.
Ziętala, M., T. Durejko, M. Polański, I. Kunce, T. Płociński, W. Zieliński, M. Łazińska, W. Stępniowski, T. Czujko and K. J. Kurzydłowski (2016). "The microstructure, mechanical properties and corrosion resistance of 316 L stainless steel fabricated using laser engineered net shaping." Materials Science and Engineering: A **677**: 1-10.
Zinoviev, A., O. Zinovieva, V. Ploshikhin, V. Romanova and R. Balokhonov (2016). "Evolution of grain structure during laser additive manufacturing. Simulation by a cellular automata method." Materials & Design **106**: 321-329.
Zinovieva, O., A. Zinoviev and V. Ploshikhin (2018). "Three-dimensional modeling of the microstructure evolution during metal additive manufacturing." Computational Materials Science **141**: 207-220.